ELSEVIER

Journal of Alloys and Compounds 456 (2008) 413–418

Journal of ALLOYS AND COMPOUNDS

www.elsevier.com/locate/jallcom

Effect of electro-discharging on formation of biocompatible layer on implant surface

Sung-Long Chen [a], Ming-Hong Lin [a], Chang-Chih Chen [b,c], Keng-Liang Ou [c,d,*]

[a] *Department of Mechanical Engineering, National Kaoshiung University of Applied Sciences, Kaoshiung 807, Taiwan*
[b] *Department of Emergency Medicine, Mackay Memorial Hospital, Taipei 110, Taiwan*
[c] *School of Dentistry, College of Oral Medicine, Taipei Medical University, Taipei 110, Taiwan*
[d] *Graduate Institute of Oral Sciences, College of Oral Medicine, Taipei Medical University, Taipei 110, Taiwan*

Received 13 October 2006; received in revised form 11 February 2007; accepted 12 February 2007
Available online 16 February 2007

Abstract

This investigation elucidates the biocompatibility and microstructural variation of Fe–Al–Mn and electro-discharged Fe–Al–Mn alloys. A recast layer was formed on the alloy surface, following electro-discharged machining. γ-Phase and $Fe_{0.6}Mn_{5.4}C_2$ carbide (κ-carbide) were formed on the recast layer following electro-discharging. The γ-phase and κ-carbide are nanostructures. The nano-(γ-phase + κ-carbide) has important roles in forming nanostructured oxide layer. Furthermore, electro-discharging not only generates a nanostructural recast layer, but also converts the alloy surface into a nanostructured oxide surface, increasing the alloy biocompatibility.

Keywords: Fe–Al–Mn; Recast layer; Electro-discharging; Biocompatibility

1. Introduction

Ferrous-based alloys, including Fe–Ni–Cr and Fe–Al–Mn, are adopted extensively in such orthopedic and dental implants because of their favorable mechanical characteristics and excellent biocompatibility. A dense oxide layer is the main factor resulting in the excellent biocompatibility. The oxide layer is always present in oxidizing media as in the human body fluid, and rebuilt in milliseconds after damaging. Hence, the tissue around an implant is in contact with the native oxide layer and not with the metal or metal alloys itself. Although commercial ferrous-based implants with native oxide films that are only 5 nm thick have exhibited long-term clinical success, situations may exist in which an implant must be modified to accelerate integration [1–10]. As ferrous-based alloys applied for biomedical application are always covered with a dense oxide film, the properties of the oxide film determine the corrosion capability of the metal-based alloys. However, body fluids contain amino acids and proteins that tend to accelerate corrosion [11]. Metallic ion release results in the poor osseointegration and often induces clinical failure. Although the fact that metallic ion release may be harmful, metals should be used because of their better strength. Accordingly, their corrosion resistance and bioactive properties should be improved. Formation of a thick oxide films on the implant surface is believed to be a prerequisite for bioactivity. Oxide films can be used as apatite inducer and providing apatite nucleation. In addition, a porous and thick oxide surface could induce bony ingrowth into the porous structure and result in morphological fixation of the implants to bone [7–12]. Porous-oxidation layers are commonly formed on the surfaces of alloy implants, passivating and fixing the implants to bone via bony ingrowths into the porous structure, promoting osseo/osetointegration [8–10]. A porous and passivated layer is typically prepared by immersion in an alkaline and/or acid solution for long period. However, such a surface modification is not efficient for fabrication. Electro-discharge machining (EDM) technology has been extensively adopted to cut and modify properties of materials [12–18]. Additionally, a machined surface modified by EDM using a silicon electrode exhibits excellent corrosion and wear resistance [19]. Microstructural variations on alloy surface by EDM have recently been examined

* Corresponding author at: Graduate Institute of Oral Sciences, College of Oral Medicine, Taipei Medical University, Taipei 110, Taiwan.
Tel.: +886 2 27361661x5400; fax: +886 2 27362295.
E-mail address: klou@tmu.edu.tw (K.-L. Ou).

0925-8388/$ – see front matter © 2007 Elsevier B.V. All rights reserved.
doi:10.1016/j.jallcom.2007.02.055

and discussed [12–19]. As described above, EDM is believed to be useful for machining implants and modifying their surfaces in situ. This study develops and elucidates a new procedure for generating nanostructural surfaces. Electro-discharging was employed to treat the Fe–Al–Mn surface. The specimens were evaluated by material analysis to determine the properties of treated and untreated Fe–Al–Mn alloys. Furthermore, the biocompatibility of the alloy with and without treatments was also investigated clearly.

2. Experimental procedure

Fe–Al–Mn alloy was prepared in an air induction furnace by conventional ingot processing using 99.5% iron, 99.7% aluminum and 99.9% manganese. Following casting, sheets of approximately 1 mm thick were cut-off directly from the ingot. Some specimens of Fe–Al–Mn alloy were electro-discharge machined using kerosene with a copper electrode and various I_p (pulse electrical current). Surface morphologies of the specimens after treatments were analyzed by scanning electron microscopy (SEM, JEOL JSM6400). In order to realize the microstructure variations, X-ray diffractometry (XRD) was carried out for phase identification. The incident angle of X-ray was fixed at three degrees. X-ray diffractometer with Cu Kα radiation operated at 50 kV and 250 mA. The phase transformation of the specimens after treatments was examined by transmission electron microscopy (TEM). Cross-sectional TEM samples were prepared electron transparency by mechanical thinning followed by ion milling in a precision ion polishing system (PIPS). Additionally, the early phase of cell–implant interactions was studied by performing a kinetic morphological analysis of the adhesion, spreading and proliferation of NIH3T3 cells to determine the biocompatibility of treated and untreated Fe–Al–Mn. The culture periods were 4 h, 8 h, 1 day, 2 days, 3 days, 5 days and 7 days, respectively. The morphology and proliferation of the cells were examined by scanning electron microscopy (SEM). The *t*-test was applied to determine the significance of the observed differences between the percentages of cells attached to Fe–Al–Mn and of those attached to surface-modified Fe–Al–Mn alloys. Each statistical test has an associated null hypothesis, and the *p*-value is the probability that the sample was drawn from the populations that are being tested. A *p*-value of 0.05 indicates that the probability of drawing the tested sample is only 5% if the null hypothesis is actually true.

3. Results and discussion

Fig. 1 displays the cross-sectional SEM morphology of electro-discharged Fe–Al–Mn alloy. The recast layer is microscale. This result is similar to the results of Lim et al. [19]. The thickness of the recast layer is associated with the field-assisted migration of ions in dielectric fluid systems. Solidified layer and molten alloy are formed rapidly as the field-assisted migration of ions proceeds continuously.

Fig. 2 presents XRD spectra of treated and untreated Fe–Al–Mn alloy. The alloy that had not undergone electro-discharging yields only γ-phase peak reflections and its structure is crystalline. Additionally, numerous reflection peaks, excluding γ-phase peaks, are obtained from the treated alloy. The crystalline structure of electro-discharged Fe–Al–Mn consists of a γ-phase and $Fe_{0.6}Mn_{5.4}C_2$ (κ) carbide, revealing that carbon saturates the γ-phase and that a larger thermal gradient is associated with the formation of saturated carbide. The above investigation demonstrates that the recast layer was formed by the molten metal with high electro-discharging energy. The electro-discharging energy may dissolve and impact more carbon and/or carbon species from the dielectric fluid as the electro-discharging energy increases, and cause the formation of

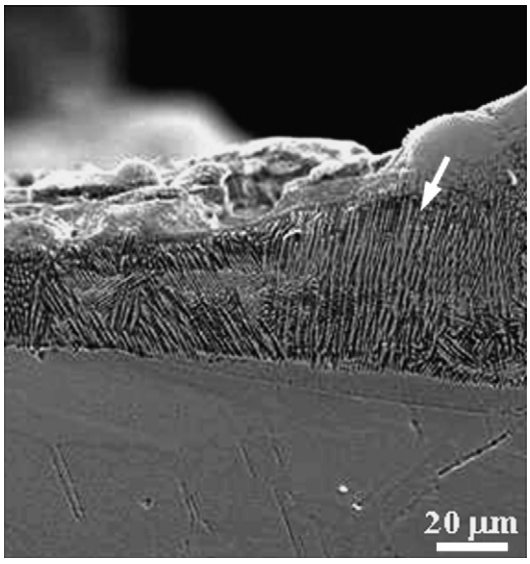

Fig. 1. Cross-sectional SEM morphology of electro-discharged Fe–Al–Mn alloy.

super-saturated γ-phase and more carbides on the rapid cooling alloy surface. During electro-discharging treatment, a chemical reaction of the equivalent activation energy is conducted to overcome the surface activation energy. This equivalent activation energy from the etchant is called the etchant activation energy (EAE). In the electro-discharging reaction, the etchant activation energy is the redox potential in the etching reaction of alloy in electrolyte. The surface activation energy acts as a barrier. Only when the etchant activation energy exceeds the surface activation energy can the reaction proceed. The alloy surface without electro-discharging initially has higher surface activation energy than the alloy surface with electro-discharging. The formation of κ-carbide and phase transformation from γ-phase to κ-carbide is associated with the thermal gradient during electro-discharging. It is believed that surface activation energy can be effectively decreased as formation of $Fe_{0.6}Mn_{5.4}C_2$ carbide. Additionally, the formation of nanostructural κ-carbide increases the grain boundaries and sub-grain boundaries on the alloy matrix, reducing the surface activation energy.

Fig. 3 displays TEM micrographs and selected area diffraction patterns (SADP) of treated and untreated Fe–Al–Mn alloy.

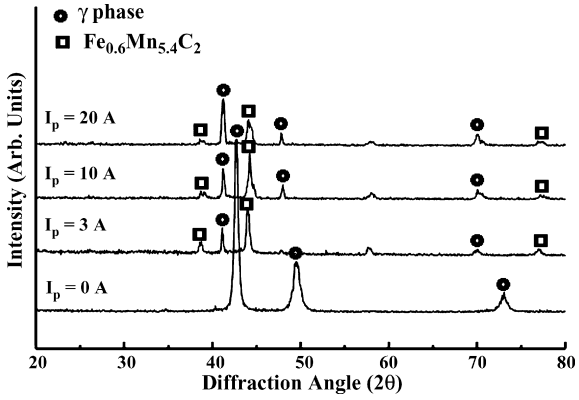

Fig. 2. XRD spectra of treated and untreated Fe–Al–Mn alloy.

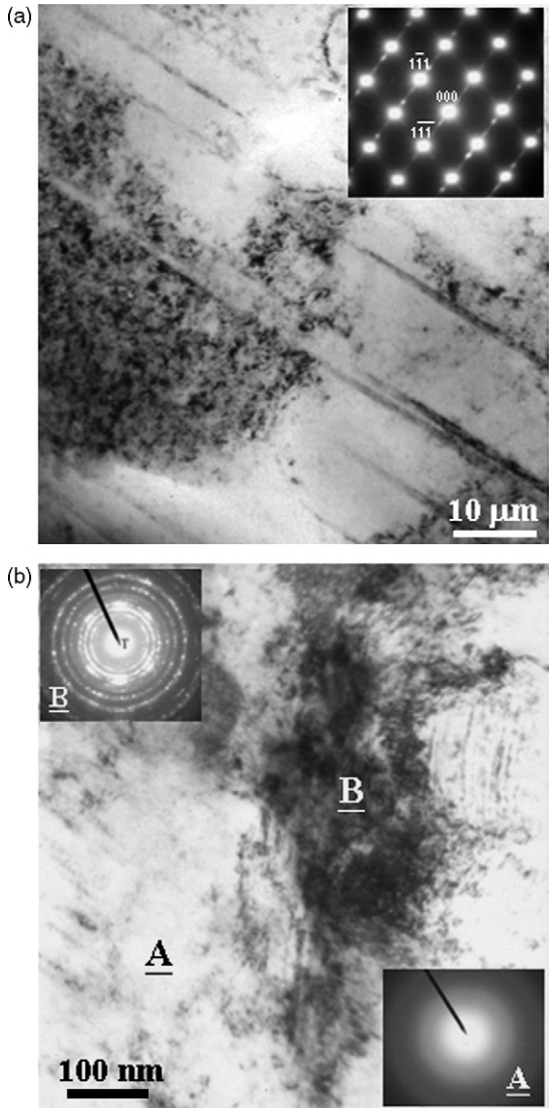

Fig. 3. TEM micrographs and selected area diffraction patterns (SADP) of treated and untreated Fe–Al–Mn alloy.

Fig. 3(a) shows a bright-field electron micrograph of the untreated alloy, which was taken from the austenite matrix of the untreated alloy under two-beam condition in the [0 0 1] zone, revealing the presence of the modulated structure within the matrix. Only austenite matrix with numerous annealing twins could be examined, as illustrated in Fig. 3(a). Fig. 3(b) presents a bright-field image and SADP of treated Fe–Al–Mn alloy. The figures demonstrate the presence of various microstructures in the alloy matrix. Fig. 3(b) also depicts an SADP of an area denoted as A. No diffraction spot is obtained from area A, indicating that the amorphous glass metal was formed on the recast layer. The diffraction ring pattern is an electron diffraction pattern, instead of a pattern of non-diffraction spots, from the area (B), revealing that the B-area is a nanostructure. From the camera length and d-spacings of the reflection spots, the crystal structure of the plate-like precipitate was determined to be $Fe_{0.6}Mn_{5.4}C_2$ having a hexagonal structure with lattice parameter $a = 5.77$ nm and $c = 6.98$ nm. Therefore, the as-treated microstructure of the alloy was austenite phase containing fine κ-carbide. Therefore, the microstructure of an electro-discharged alloy was a mixture of nano-(γ-phase + κ-carbide). The grain size of the carbides was only 20 nm, indicating that not only was the nanophase formed during electro-discharging reactions, but also electro-bombardment was responsible for nanocrystallization. As stated above, during electro-discharging, nucleation and growth solidified liquid metals, and over cooling can stabilize nucleation and control the nucleation rate. Liquid metals are easily nucleated, preventing them from becoming metal glass, because they are more viscous and crystallize fast. An amorphous metal must typically have a high cooling rate [20]. Phase transformation during supercooling is responsible for the complex microstructures in the recast layer.

Fig. 4 presents the SEM photographs of the Fe–Al–Mn alloy with and without EDM. Fig. 4(a) presents the untreated alloy surface. It is not observably porous. Only machined textures were observed on the surface. The porous structure is gen-

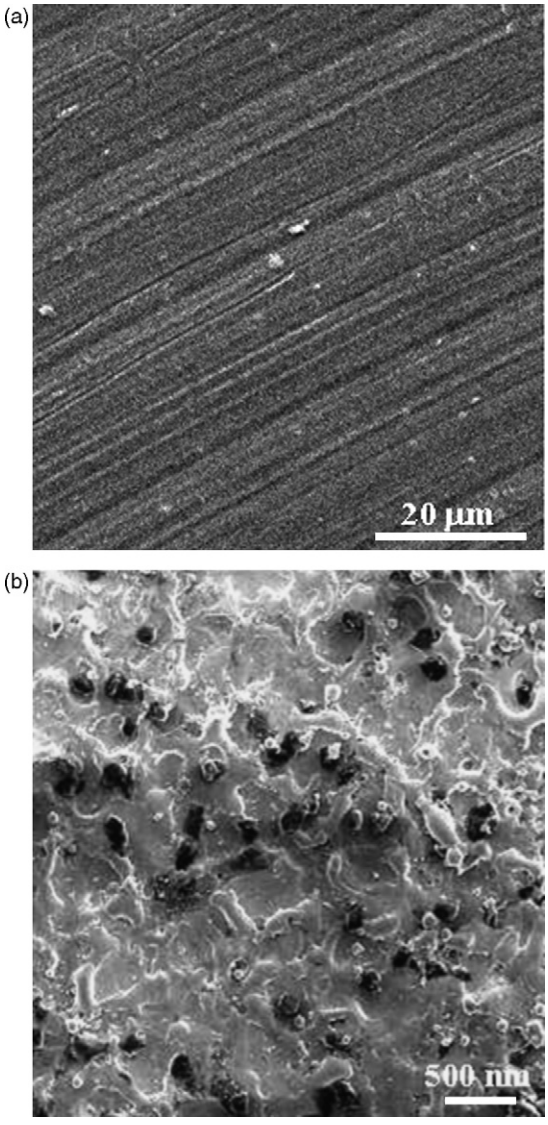

Fig. 4. Highly magnified SEM image Fe–Al–Mn alloy: (a) without treatment, and (b) with treatment.

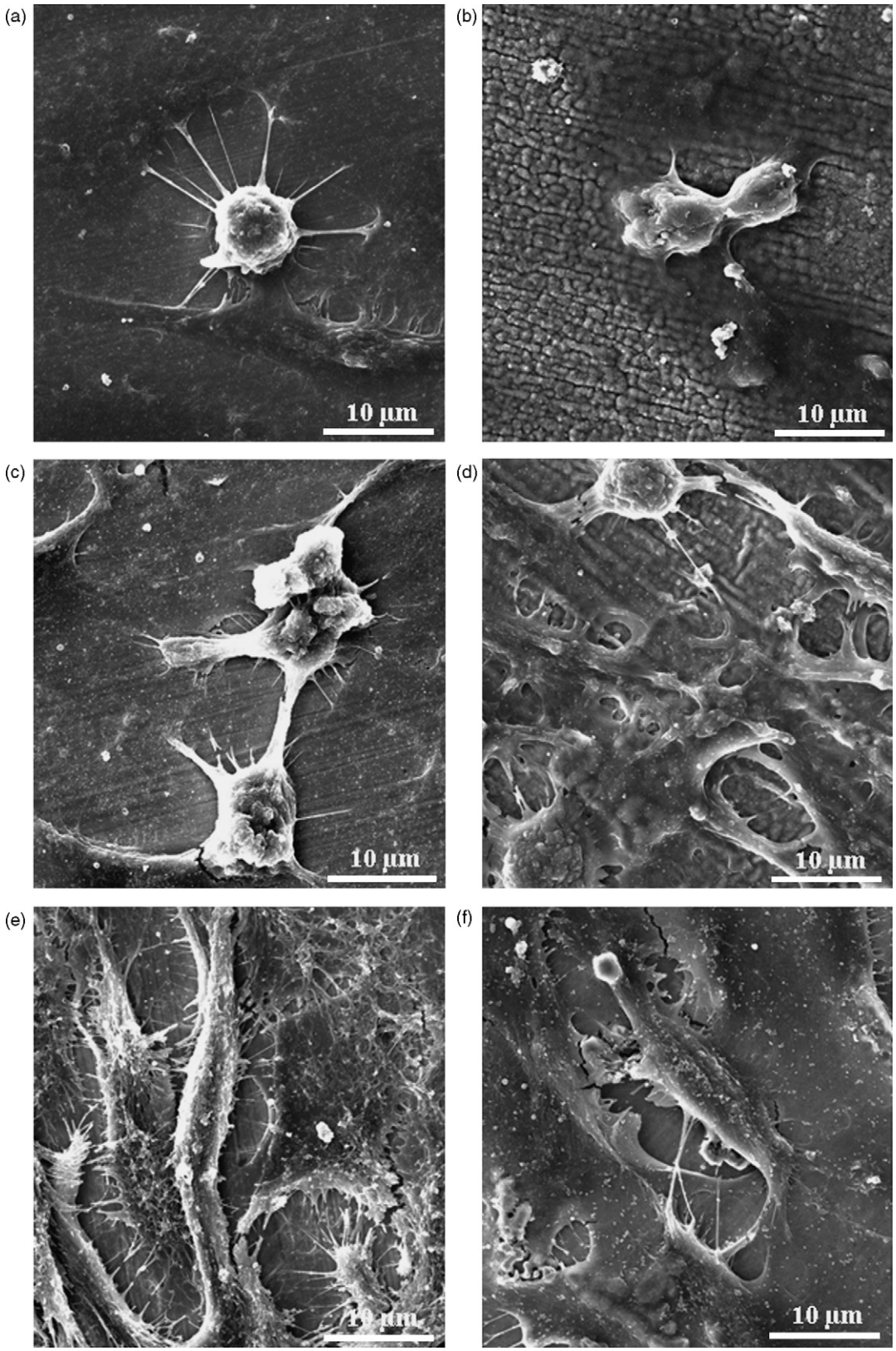

Fig. 5. SEM micrographs demonstrating cellular morphology of treated and untreated Fe–Al–Mn alloy after various culture times: (a and b) 8 h, (c and d) 24 h, and (e and f) 48 h.

erally obtained by extended immersion in chemical solution [7–10]. Nanoporous structures and the volcano-like and re-solidified molten metals were observed on the EDM-treated surface. Fig. 4(b) presents the nanoporous structure and thick oxide layer. As is widely believed, the thicker oxide layer and porosity are responsible for the improved implant performance.

The SEM investigations of cell morphology on Fe–Al–Mn alloys with and without treatments are shown in Fig. 5. Cells spread effectively on treated and untreated alloy following various culturing periods, suggesting favorable attachment and biocompatibility. The cells fully adapted to the treated and untreated Fe–Al–Mn alloys. After 8 h of cell culture, SEM examination demonstrated that the cells on treated and untreated Fe–Al–Mn alloys were round with central, protruding nuclei that were surrounded by a thin rim of cytoplasm (Figs. 5(a and b)). Fig. 5(c and d) present cell surface morphology on treated and untreated Fe–Al–Mn alloys after culturing for 24 h, respectively. Protruding nuclei can still be observed on the cells on untreated Fe–Al–Mn alloy, even though some cells were flat, well-spread and polygonal. Furthermore, the cells on the treated alloys surfaces have no clear orientation. The cells were flat, well spread and clearly polygonal without protruding nuclei. After culturing for 24 h, the cells were more elongated than after culturing for 12 h. After 48 h of culturing on untreated Fe–Al–Mn alloy, as displayed in Fig. 5(e), most of the cells had begun to grow along the machined tracks and fine irregularities. Moreover, most had begun to differentiate along the fine irregularities after 48 h of culture, as displayed in Fig. 5(f), and the cultured cells were strongly attached, elongated, flat and irregularly networked, indicating that the treated Fe–Al–Mn alloy had greater biocompatibility than untreated Fe–Al–Mn alloy. On the treated Fe–Al–Mn alloy, the cells were mostly polygonal, flat and well spread, without a particular orientation. The volcano-like and non-volcano-like surface as re-solidified molten metal exhibited a single behavior. Several filopods were present. The cells on the treated alloy were more widely dispersed and had more, longer filpods than those on the untreated alloy. Moreover, the nanoporous structure had a greater effect on the cell morphology of the electro-discharged alloy than on that of the treated alloy. The cells had a nanoporous, molten and re-solidified surface, probably because of the greater contact area on the treated surface than on the untreated surface, which is associated with an increased capacity for cell proliferation and differentiation.

Fig. 6 presents the cell counting results for treated and untreated Fe–Al–Mn. The cell reactions following seeding included anchorage, attachment, adhesion, migration and cell division. After 4 h of culture, the cells were attached and adherent, but not significantly spread. The attachment of bone-derived cells associated quantity varied only slightly the dispersion of the attached cells. After 8 h of culture, the cells had spread to virtually all of the studied surfaces. More cells attached to the electro-discharged Fe–Al–Mn than to the pure Fe–Al–Mn. The attachment assay with 24 h culture indicated that significantly ($p < 0.05$) more cells attached to the electro-discharged Fe–Al–Mn than to the pure Fe–Al–Mn. After 48 h of culture, more cells had attached to the electro-discharged Fe–Al–Mn surfaces. The percentage of cells that were attached substantially

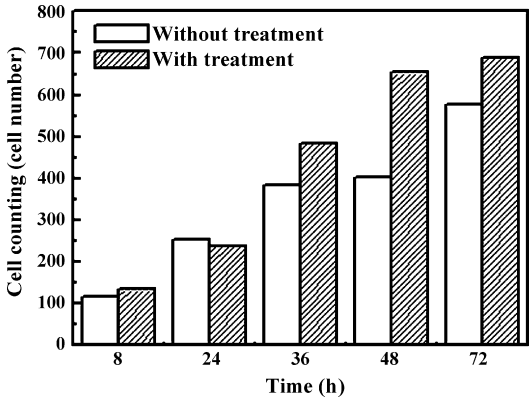

Fig. 6. Cell counting results for Fe–Al–Mn with and without EDM treatments.

exceeded that attached to the untreated Fe–Al–Mn. As described above, the cells spread on electro-discharged Fe–Al–Mn more rapidly than on pure Fe–Al–Mn. Moreover, the cells on the treated surfaces took less time to reach confluence. The results of the MTT assay with serial dilutions of extracts of the electro-discharged Fe–Al–Mn alloy on 3T3 cells were also considered. The MTT assay demonstrated that significantly ($p < 0.05$) more cells were attached to the electro-discharged Fe–Al–Mn. A difference between the biocompatibility with osteoblasts of surface-treated and untreated alloy is observed. Surface properties of implants must probably be modified in a careful and controlled manner [9–12,21]. Implants such as dental implant and mini-implant are well known to be highly biocompatible. Modifying the surfaces of the metal-based implants improved their functionality and biocompatibility. Hence, metal-based implants are recommended for use as coatings on blood-contacting implants. The adhesion of blood cells on various implants with smooth and rough surfaces following surface treatment has been discussed elsewhere [22,23]. Cell adhesion was higher on rougher surfaces, with a Ra in the range 0.2–0.5 mm [24]. Additionally, a nitrided implant exhibits substantially higher human salivary albumin adsorption, indicating the high affinity of human albumin for implants [25]. The recast layer with κ-carbide was demonstrated to mainly comprise C–C or C–H bonds (hydrocarbons) with minor fractions of C–O, C=O, and C–OH bonds in biological environment. The recast layer, containing nano-κ-carbide, brought about more amine and carboxyl groups produced on the implant surfaces. It is believed that the recast layer is suitable for raising the concentration of reactant molecules and functional groups. As described above, variations in surface characteristics due to surface modifications importantly influence biocompatibility.

4. Conclusion

The effectiveness of electro-discharging on the surface modification of Fe–Al–Mn alloy has been examined. A nanostructural recast layer was formed by electro-discharging field migration and ion bombardments. In the recast layer, nano-$Fe_{0.6}Mn_{5.4}C_2$ having a hexagonal structure with lattice parameter $a = 5.77$ nm and $c = 6.98$ nm was investigated. Furthermore, in the austenite matrix, a $\gamma \rightarrow \kappa$-carbide ordering transition would occur during

electro-discharging. Therefore, the as-treated microstructure of the alloy was austenite phase containing fine κ-carbide. Nano-($\gamma + \kappa$-carbide) phases were formed by electro-discharging. The formation of nanostructural recast layer is important in improving the biocompatibility of alloys. The phase transformation of Fe–Al–Mn alloy following electro-discharging is posited to be crucial in increasing the biocompatibility and osseo/osetointegration of Fe–Al–Mn alloys.

Acknowledgement

The authors would like to thank the National Science Council of Republic of China for financially supporting this research under Contract No. NSC-94-2212-E-151-005 and NSC-94-2314-B-038-032.

References

[1] M. Long, H.J. Rack, Biomaterials 19 (1998) 1621.
[2] B. Kasemo, J. Prosthet. Dent. 49 (1983) 832.
[3] D.F. Williams, J. Med. Eng. Technol. 1 (1977) 266.
[4] R. Adell, Int. J. Oral Maxillofac. Implant. 5 (1990) 347.
[5] X.X. Wang, S. Hayakawa, K. Tsuru, A. Osaka, Biomaterials 23 (2002) 1353.
[6] Y.C. Shyng, H. Devlin, K.L. Ou, Int. J. Prosthet. 19 (5) (2006) 513.
[7] H.C. Cheng, S.Y. Lee, C.M. Tsai, C.C. Chen, K.L. Ou, Electrochem. Solid-State Lett. 9 (2006) D25.
[8] H.C. Cheng, S.Y. Lee, C.C. Chen, Y.C. Shyng, K.L. Ou, Appl. Phys. Lett. 89 (2006) 173902-1.
[9] Y.H. Shih, C.T. Lin, C.M. Liu, C.C. Chen, C.S. Chen, K.L. Ou, Appl. Surf. Sci. 253 (2007) 3678.
[10] H.C. Cheng, S.Y. Lee, C.C. Chen, Y.C. Shyng, K.L. Ou, J. Electrochem. Soc. 154 (1) (2007) E13.
[11] K. Merritt, S.A. Brown, J. Biomed. Mater. Res. 22 (1988) 111.
[12] H.M. Kim, T. Kokubo, S. Fujibayashi, S. Nishiguchi, T. Nakamura, J. Biomed. Mater. Res. 52 (2000) 553.
[13] F. Klocke, D. Lung, G. Antonoglou, D. Thomaidis, J. Mater. Process. Technol. 149 (2004) 191.
[14] H.G. Lee, J. Simao, D.K. Aspinwall, R.C. Dewes, W. Voice, J. Mater. Process. Technol. 149 (2004) 334.
[15] W.S. Zhao, Q.G. Meng, Z.L. Wang, J. Mater. Process. Technol. 129 (2002) 30.
[16] Y.H. Guu, H. Hocheng, Mater. Manuf. Process. 16 (1) (2001) 91.
[17] Y.C. Lin, B.H. Yan, Y.S. Chang, J. Mater. Process. Technol. 104 (2000) 171.
[18] Y.S. Wong, L.C. Lim, I. Rahuman, W.M. Tee, J. Mater. Process. Technol. 79 (1998) 30.
[19] L.C. Lim, L.C. Lee, Y.S. Wong, H.H. Lu, Mater. Sci. Technol. 7 (1991) 239.
[20] P. Duwez, ASM Trans. 60 (1967) 607.
[21] B.D. Ratner, J. Biomed. Mater. Res. 27 (1993) 837.
[22] J.Y. Park, C.H. Gemmell, J.E. Davies, Biomaterials 22 (2001) 2671.
[23] S.I. Tanaka, M. Aonuma, N. Hirose, T. Tanaki, J. Electrochem. Soc. 11 (2002) 167.
[24] M.F. Maitz, M.T. Pham, E. Wieser, I. Tsyganov, J. Biomater. Appl. 17 (2003) 303.
[25] M.C. Sunny, C.P. Sharma, J. Biomater. Appl. 6 (1991) 89.